Shock-Wave-Boundary-Layer Interaction Effects on Aerodynamic Heating

F. T. Hung,* S. N. Greenschlag,* and C. A. Scottoline†
Rockwell International Corporation, Downey, Calif.

A simple method is developed to predict heating to a flat plate surface influenced by an impinging shock wave emanating from a two-dimensional wedge. Once the freestream flow conditions and shock generator wedge angle are specified, peak heating values can be computed for either laminar or turbulent oncoming flow. Flow that is initially laminar can either remain laminar or be tripped to transitional or turbulent flow by the impinging shock wave. A transition Reynolds number for flow perturbed by the impinging shock wave is also derived from heating correlations. Finally, the study results indicate that the extremely large increases in interference heating over the undisturbed flat plate values are partially due to boundary-layer transition caused by the impinging shock wave. Experimental data obtained from simple geometry wedge/flat plate models as well as recent results from Space Shuttle models are used in this analysis.

Nomenclature

A,a,b,C	= constants
Cp	= constant pressure specific heat
H	= convective heat-transfer coefficient
L	= Space Shuttle Orbiter fuselage or external tank reference length
ℓ	= distance measured from Space Shuttle Orbiter or external tank nose
M	= Mach number
p	= pressure
Pr	= Prandtl number
r	= recovery factor
Re	= Reynolds number
Re/ft	= unit Reynolds number
St	= Stanton number
T	= temperature
V	= velocity
x	= distance measured from flat plate leading edge
x_{PK}	= distance from flat plate leading edge to peak interference heating location (Fig. 6)
α	= Space Shuttle angle of attack
β	= Space Shuttle yaw angle
δ	= wedge angle
γ	= specific heat ratio
ρ	= density

Superscript

*	= Eckert reference conditions

Subscripts

∞	= freestream
1	= flow region behind impinging shock wave
2	= flow region behind reflecting shock wave
c	= computed
e	= boundary-layer edge conditions
ET	= Space Shuttle external tank
FS	= Space Shuttle Orbiter fuselage
i	= interference
m	= measured
o	= stagnation
PK	= peak
r	= recovery
ref	= stagnation point of a sphere (1-ft radius for wedge/flat plate case and scaled 1-ft radius for Space Shuttle case)
trans	= transition
u	= undisturbed flow
w	= wall conditions

Presented as Paper 76-355 at the AIAA 9th Fluid and Plasma Dynamics Conference, San Diego, Calif., July 14-16, 1976; submitted July 21, 1976; revision received Oct. 15, 1976.

Index categories: LV/M Aerodynamic Heating; Jets, Wakes, and Viscid-Inviscid Flow Interactions; Supersonic and Hypersonic Flow.

*Member of the Technical Staff, Aero Sciences Department, Space Division.

†Supervisor, Aero Sciences Department, Space Division.

Introduction

AERODYNAMIC heating has been a major concern for designers of supersonic or hypersonic vehicles, since the thermal protection system and consequently the weight of the vehicle are related to the heating experienced. Heating problems can be even more severe if the vehicle surface is subjected to impinging shock waves or if its smoothness is marred by protuberances, cavities, gaps, etc. Shock-wave impingement can create very high local heating on the vehicle surface, which is the subject of this study.

Typical shock-impingement heating data from Ref. 1 is shown in Fig. 1. For a freestream Mach number of 8, a shock wave emanating from a 15° wedge impinges on a flat plate and interacts with the boundary layer on the plate. Thermocouple measurements indicate that the peak interference heat-transfer coefficient on the plate, $H_{i,PK}$, can be 128.8 times as high as the undisturbed value (flat plate without wedge) measured at the same location, H_u. However, as will be discussed later, these large factors are typical of situations where the shock impingement has tripped the laminar oncoming flow to turbulent. The reference heat-transfer coefficient, H_{ref}, in Fig. 1 is the stagnation point value of 1-ft radius sphere computed with the Fay-Riddell equation.

For a typical Space Shuttle configuration, as shown in Fig. 2, experimental results[2] also show severe interference heating as indicated in Figs. 3 and 4. The orbiter nose bow shock impinges and interacts with the external tank (ET) boundary layer and causes high heating with a value of $H_{i,PK}/H_u$ of 14.5 as indicated in Fig. 3. The impinging shock wave on the ET is then reflected back on the orbiter lower surface as shown in Fig. 4 and causes interference heating with a $H_{i,PK}/H_u$ value of 15. The presence of a support strut in the region of reflecting shock impingement complicates the orbiter case. However, the basic phenomenon is the same. It should be noted that heating data in Figs. 3 and 4 are taken at

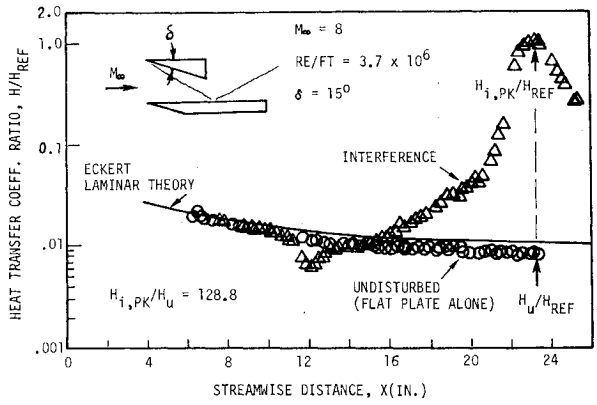

Fig. 1 Typical wedge/flat-plate interference heating data.[1]

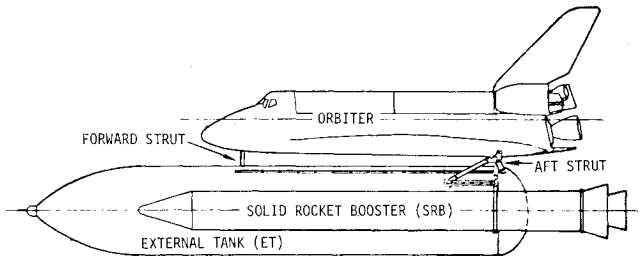

Fig. 2 Space Shuttle configuration.

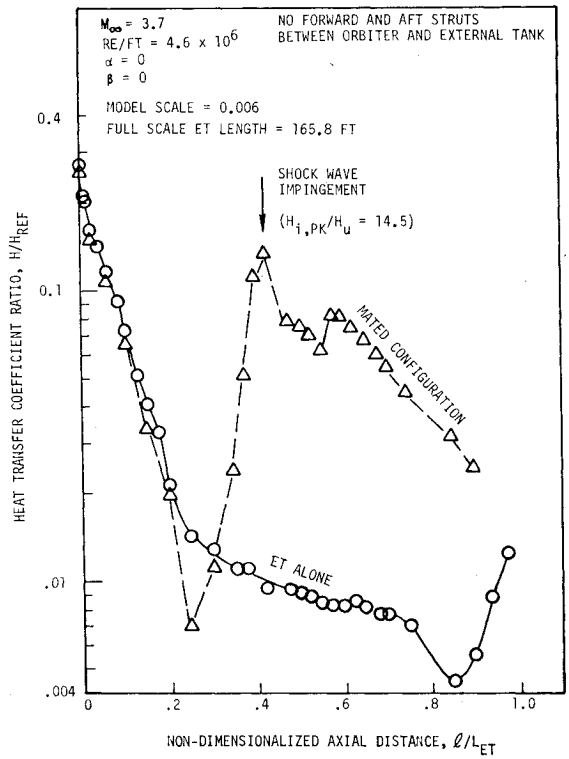

Fig. 3 Heating on Space Shuttle external tank upper centerline.[2]

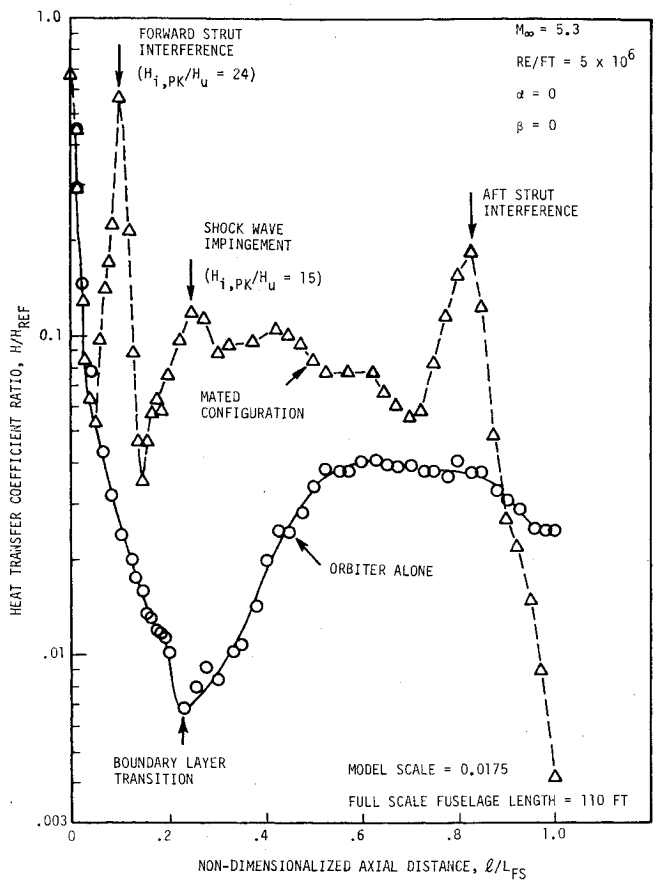

Fig. 4 Heating on Space Shuttle Orbiter lower centerline.[2]

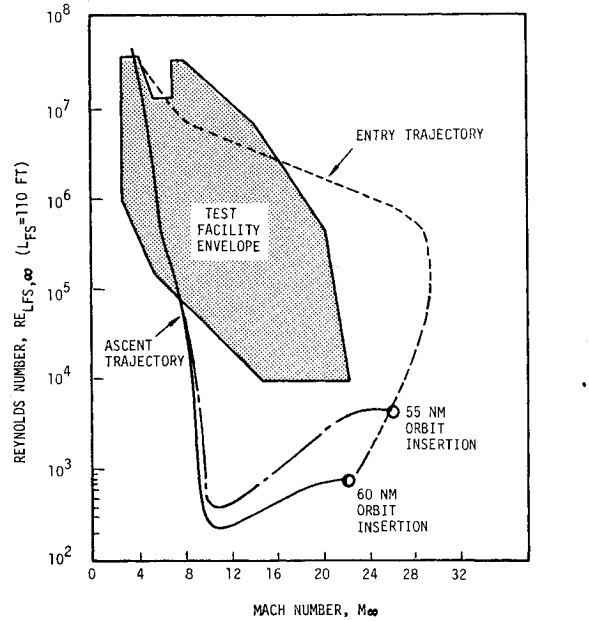

Fig. 5 Space Shuttle flight trajectories and wind-tunnel test facility envelope.[2]

a relatively low Mach number. Peak interference heating factors $H_{i,PK}/H_u$ can be even higher at higher Mach numbers, since it is well known that shock-impingement heating increases with Mach number.

During recent years Space Shuttle-related aerodynamic heating experiments have been conducted at many different test facilities with different model scales, configurations, and flow conditions. The overall test envelope is compared with Shuttle flight trajectories in Fig. 5. The comparison indicates that flight trajectories cannot be completely simulated by ground tests. Cost considerations also limit the amount of data that can be obtained. Consequently, methods must be developed to extend existing experimental data to any Mach number and Reynolds number along a flight trajectory.

An approach to analyzing and eventually predicting peak shock impingement heating can be either analytic or experimental. The complexities involved in shock wave/boundary-layer interaction make an analytical approach quite difficult. For instance, the oncoming undisturbed flow can be

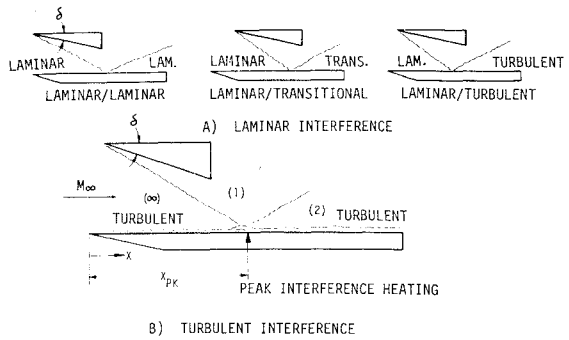

Fig. 6 Wedge/flat-plate model and definition of symbols.

laminar or turbulent. The laminar flow may be tripped by the impinging shock wave and become transitional or turbulent as shown in Fig. 6. Also, the boundary layer can be either separated or attached depending on shock strength. A critical review by Murphy[3] indicates that analytic methods to predict interference heating are very limited even for the simple case of a completely laminar flow. However, during the past decade, experimental investigations with two-dimensional wedge/flat-plate models have been conducted over a wide range of flow conditions and model configurations. Some of the existing data have been collected and analyzed in this study, and a simplified method has been developed that predicts peak interference heating values once the flow conditions and wedge angle are specified.

Analysis

Studies of compressible flow heat transfer[4-6] have shown that the local heat-transfer coefficient may be regarded generally as a function of several variables. In particular, the Stanton number has been shown to be a function of the local values of Reynolds number, Prandtl number, Mach number, and the ratio of wall to boundary-layer edge temperature. In obtaining the desired correlation, however, consideration must be given to coupling effects between the various dimensionless groups. Eckert[4] has shown that, in the absence of shock waves, compressible heat-transfer data may be correlated by an expression of the form

$$ST_u^* = A(Re_x^*)^a (Pr^*)^b \qquad (1)$$

where A, a, and b are constants dependent upon the flow regime. In Eq. (1), those properties used in computing the Stanton, Reynolds, and Prandtl numbers are to be evaluated at a reference temperature T^* given by

$$T^*/T_e = 1 + \tfrac{1}{2}[(T_w/T_e) - 1] + 0.22[(T_r/T_e) - 1] \qquad (2)$$

with

$$T_r/T_e = 1 + r[(\gamma - 1)/2]M_e^2 \qquad (3)$$

The Eckert reference method was first applied to predict peak laminar interference heating by Hung.[7] The interference Stanton number was correlated with Reynolds number and Prandtl number based on either upstream or downstream flow conditions. The downstream flow approach is chosen in this analysis. As discussed in Ref. 7, the shock strength term can be eliminated in the correlation when downstream flow properties are used. The proposed correlation is thus expressed in the following form

$$ST_{i,PK(2)}^* = A[RE_{X,PK(2)}^*]^a [Pr_{(2)}^*]^b \qquad (4)$$

where subscript (2) refers to the inviscid flowfield behind the reflecting shock wave as shown in Fig. 6. The collected wedge/flat-plate data[1,8-15] used in this study are summarized in Table 1. The data covers a wide range of freestream Mach numbers ($M_\infty = 2.4$-13), unit Reynolds numbers ($Re/ft = 0.4\times10^6$-36.6×10^6), running lengths ($x_{PK} = 0.38$-10.7 ft), and wedge angles ($\delta = 1$-20°) with the oncoming flow either laminar or turbulent. As will be shown later, the Eckert reference Reynolds number, based on flow conditions behind the shock, varies from 1.7×10^4 to 4×10^8 for the data studied (a range of almost five orders of magnitude). The wide range of Mach numbers and wedge angles provides a wide range of shock strengths that affect heating level and flow transition. The wide range of unit Reynolds numbers and running lengths provides a wide range of Reynolds numbers which also affect both heating level and flow transition.

Total temperature T_o total pressure P_o freestream Mach number, M_∞, flat-plate surface temperature, T_W, and wedge angle, δ, are needed to compute flow properties behind impinging and reflecting shock waves. The measured peak heat transfer coefficient, $H_{i,PK}$, is then combined with a computed value of $C_{p2}^*\rho_2^*V_2$ to form a reference Stanton number, $St_{i,PK(2)}^*$. This Stanton number is then correlated with a com-

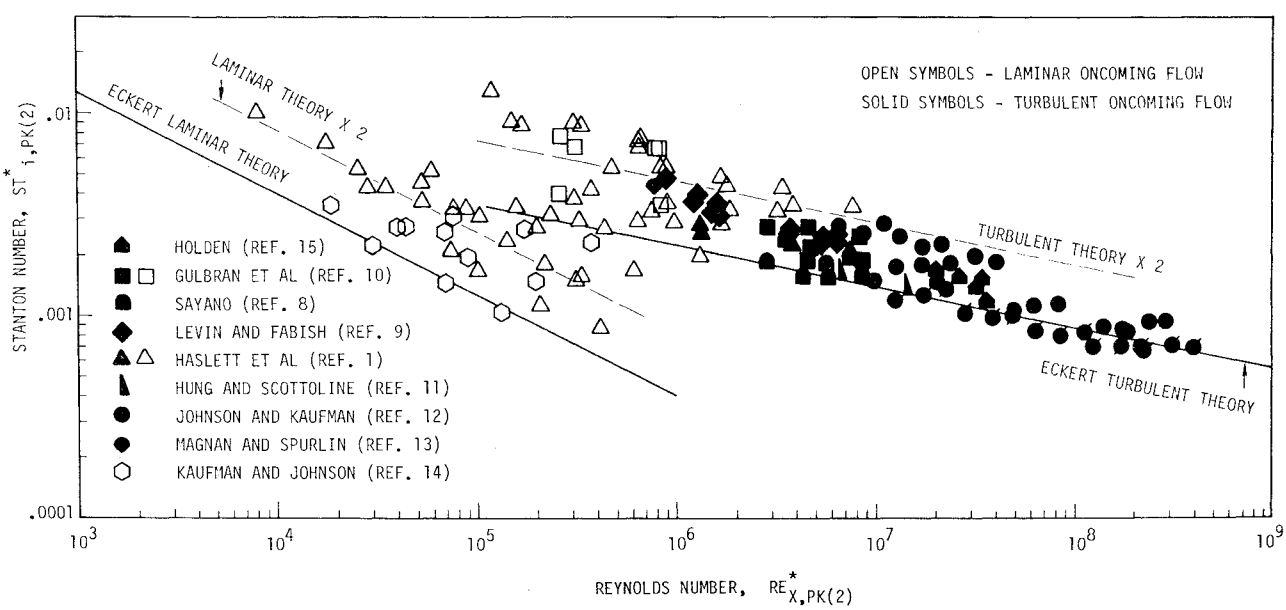

Fig. 7 Wedge/flat-plate peak interference heating data correlation – preliminary.

Table 1 Wedge/flat plate interference heating test summary

Author(s)	Ref.	M_∞	Re/ft	X_{PK}(ft)	P_0(psia)	T_0(°R)	δ(deg)
			a) Turbulent oncoming flow				
Holden	15	8.6-13.0	$4.7\text{-}11\times10^6$	2.33-3.25	4570-19900	1820-3400	12.5-20.0
Gulbran et al.	10	6-10	$2.16\text{-}3.4\times10^6$	2.0-2.83	190-1800	850-1890	10-15
Sayano et al.	8	2.4-5.0	$3.3\text{-}4.7\times10^6$	1.7	25-64	565-605	8-15
Levin and Fabish	9	2.95-5.02	$3.6\text{-}7.4\times10^6$	1.06-1.12	49-64.2	560-575	6-12
Haslett et al	1	8	3.7×10^6	1.87-1.92	850	1341	5-15
Hung and Scottoline	11	5.24	3.5×10^6	3.58	350.9-352	1473-1529	5-10
Johnson and Kaufman	12	6	$2.47\text{-}36.6\times10^6$	1.03-10.7	140-2615	855-1022	10-15
Magnan and Spurlin	13	10.2	2.16×10^6	2.33	1800	1890	5
			b) Laminar oncoming flow				
Gulbran et al.	10	6-10	1×10^6	1.55-1.83	50-750	850-1800	5-10
Kaufman and Johnson	14	8	$0.4\text{-}2.0\times10^6$	0.89-1.22	70-429	1265-1395	1-5
Haslett et al.	1	8	$0.41\text{-}3.7\times10^6$	0.375-1.93	75-850	1200-1341	1.5-15

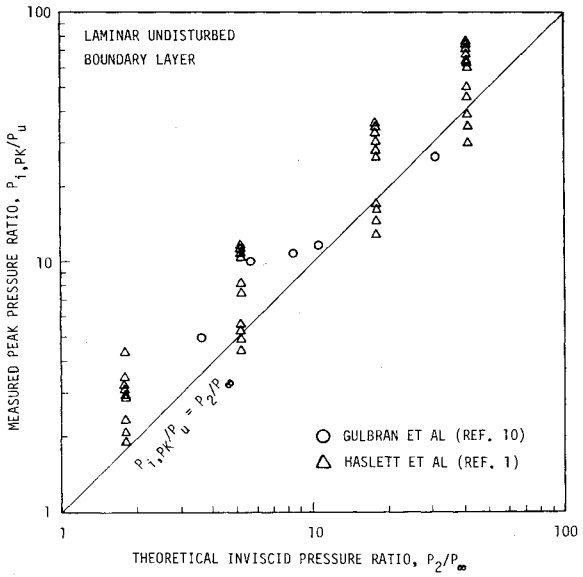

Fig. 8 Measured wedge/flat-plate interference pressure data vs computed inviscid values.

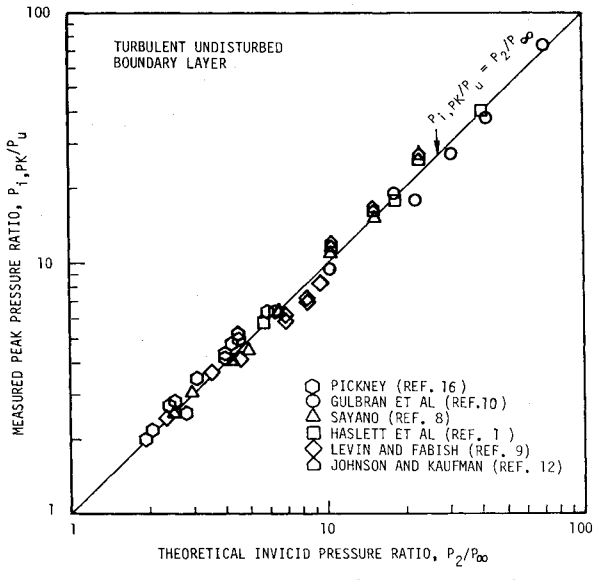

Fig. 9 Measured wedge/flat-plate interference pressure data vs computed inviscid values.

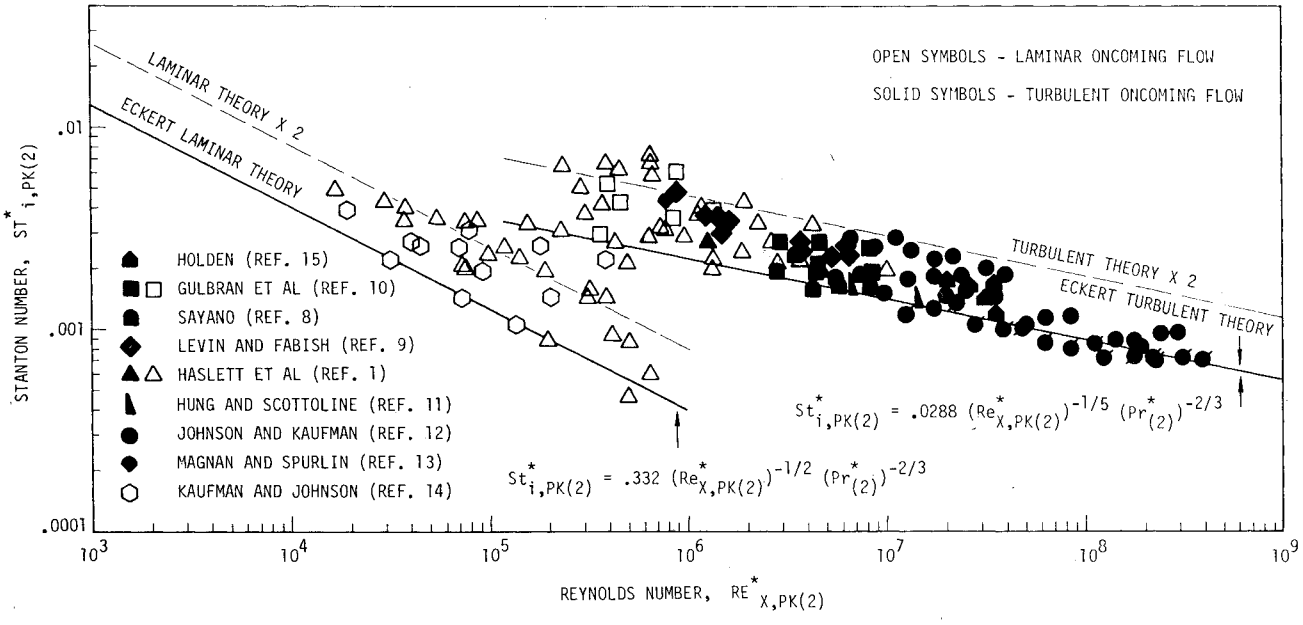

Fig. 10 Wedge/flat-plate peak interference heating data correlation – final.

puted $Re^{*}_{x,PK(2)}$ as shown in Fig. 7. Eckert's laminar and turbulent flat-plate theories are also shown for comparison purposes. The correlation in Fig. 7 should be considered preliminary since careful study of the data sources revealed that certain effects could be accounted for in order to improve the correlation as discussed in the following text.

In addition to the desired shock wave generated from the wedge, the wedge/flat-plate model usually generates additional shock waves as discussed in Ref. 1. These additional shock waves reinforce the simple wedge-generated shock wave and result in measured pressure values on the flat-plate surface that are substantially larger than those computed for the simple wedge shock as shown in Fig. 8. Part of the measured data from Ref. 1 are lower than the computed values as shown in Fig. 8. This is caused by the coalescence of the expansion fan from the wedge trailing edge and the shock wave impingement region on the flat plate as discussed in Ref. 10. This is clearly indicated in the Schlierens and shadowgraphs presented in Ref. 1, especially for the large wedge angle cases. It is expected that when no additional shock wave is present, the measured peak pressure should agree with computed inviscid value as shown in Fig. 9.

Besides additional shock waves, another cause of data deviation is the displacement thickness growth of the boundary layer on the wedge as discussed in Refs. 1 and 14. The effect is not significant for the case of large Reynolds numbers and wedge angles. However, for the case of small Reynolds numbers and wedge angles, the effect must be considered, as the effective wedge angle can be significantly larger than the actual wedge angle. This results in a stronger shock wave and consequently higher interference pressure and heating on the flat plate.

In this study, the measured peak pressure ratio, $P_{i,PK}/P_u$, was compared with the computed inviscid pressure ratio, P_2/P_∞. An effective wedge angle was computed based on $P_{i,PK}/P_u$ whenever $P_{i,PK}/P_u$ was significantly higher than P_2/P_∞ due to either an additional shock wave or the displacement thickness effect on the wedge. The modified wedge angle was then used to recompute the flow properties behind shock wave and the dimensionless groups in Eq. (4). The finalized correlation is shown in Fig. 10.

In Ref. 12, a wide range of Reynolds numbers is produced by impinging shock waves on either a flat plate as shown in Fig. 11a or on a curved wind-tunnel door with an extremely long running length as shown in Fig. 11b. Measured values of $P_{i,PK}/P_u$ on the flat plate agree well with computed values of P_2/P_∞, whereas measured values of $P_{i,PK}/P_u$ on the curved door are lower than computed P_2/P_∞ values as shown in Fig.

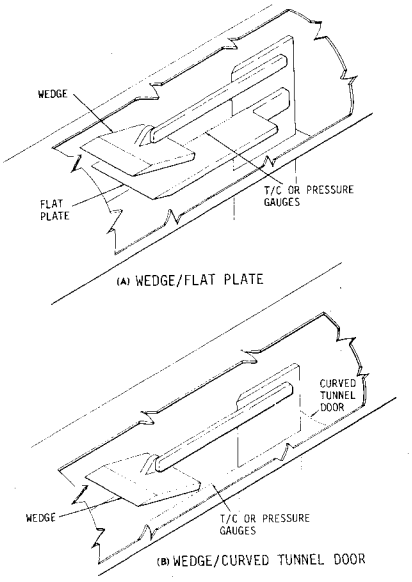

Fig. 11 Test model configurations.[12]

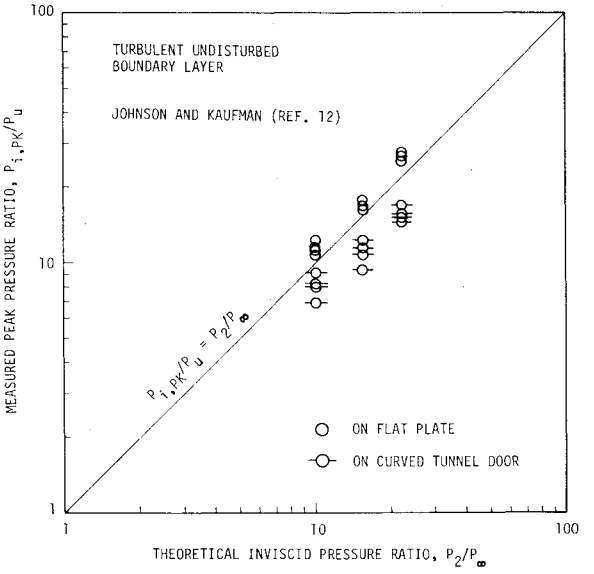

Fig. 12 Measured peak interference pressure data vs computed inviscid values.[12]

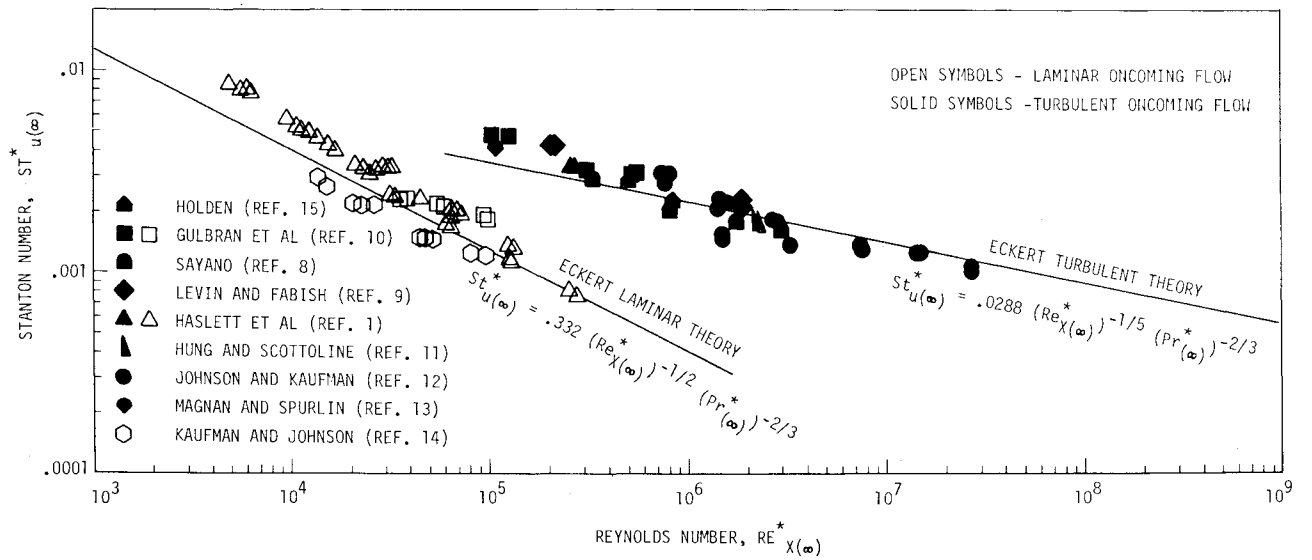

Fig. 13 Undisturbed flat-plate heating data correlation.

12. It is speculated that the lower peak pressure values on the curved door may be caused either by a thick boundary layer due to the long running length or by possible pressure relief in the lateral direction. The thick boundary layer may "smooth" the pressure distribution in the flow direction and consequently flatten the pressure peak. Also, pressure relief in the lateral direction may occur, since the planar shock wave emanating from the two-dimensional wedge impinges on the curved door at different x stations. Both actual wedge angles (solid circles) and effective wedge angles based on pressure measurements (solid circles with flags) were used in the correlations shown in Figs. 7 and 10.

Instead of actual test run values of T_o and P_o, some of the references only provide nominal values, which were used in this study. This can contribute additional data scattering in the final interference heating correlation. This error cannot be directly quantified but its effect on interference heating can be estimated by investigating the undisturbed heating data as shown in Figs. 13 and 14. Each value of H_u in these figures is the measured undisturbed value at the same location where peak interference heating occurs, i.e., H_u at x_{PK}. The data scatter in these figures could, at least partially, be the result of the unknown previously discussed.

Results and Discussion

The final peak interference heating data correlation is compared with Eckert's laminar and turbulent theories as shown in Fig. 10 where open and solid symbols are data for laminar and turbulent oncoming flow, respectively. The following conclusions can be drawn:

1) For the case of low Reynolds number, the oncoming laminar flow remains laminar in the interference region. The laminar/laminar data vary with Reynolds number in the manner as Eckert's laminar theory, i.e., $St^*_{i,PK(2)} \sim (Re^*_{x,PK(2)})^{-1/2}$.

2) At higher Reynolds numbers, the impinging shock wave trips the oncoming laminar flow and causes flow transition in the interference region. The laminar/turbulent data vary with Reynolds number in the same manner as Eckert's turbulent theory,i.e., $ST^*_{i,PK(2)} \sim (Re^*_{x,PK(2)})^{-1/5}$.

3) At even higher Reynolds numbers or with a boundary-layer trip installed near the flat-plate leading edge, the oncoming flow is turbulent and remains turbulent in the interference region. The turbulent/turbulent data also follow Eckert's turbulent heating correlation as discussed in conclusion 2.

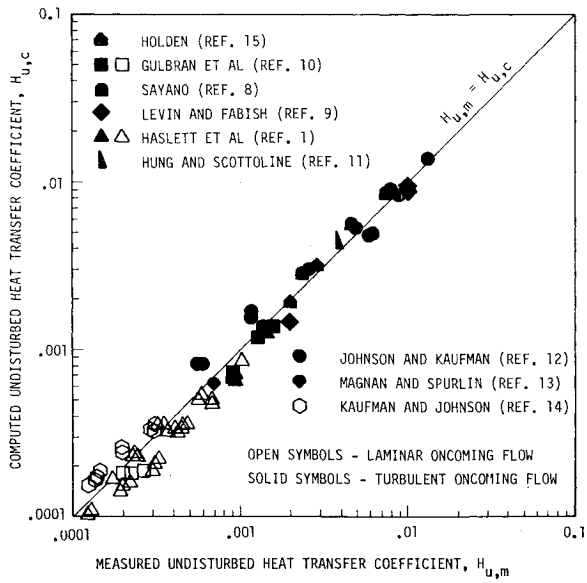

Fig. 14 Measured undisturbed flat-plate heating data vs computed values (Eckert's reference method).

4) Boundary-layer transition due to an impinging shock wave is clearly shown by comparing data with Eckert's laminar and turbulent theories. The open symbols along the laminar and turbulent theory lines are laminar/laminar and laminar/turbulent data, respectively, whereas the open symbols between the two theory lines are laminar/transitional values. The solid symbols are turbulent/turbulent data.

5) With shock impingement, boundary-layer transition occurs at a fairly low Reynolds number as shown in Fig. 10 with

$$Re^*_{\text{trans}(2)} = 10^5 - 10^6$$

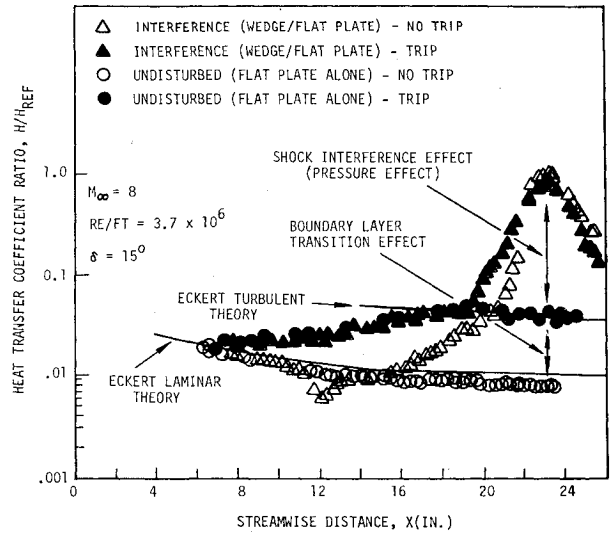

Fig. 15 Effect of boundary-layer trip on wedge/flat plate interference and undisturbed heating.[1]

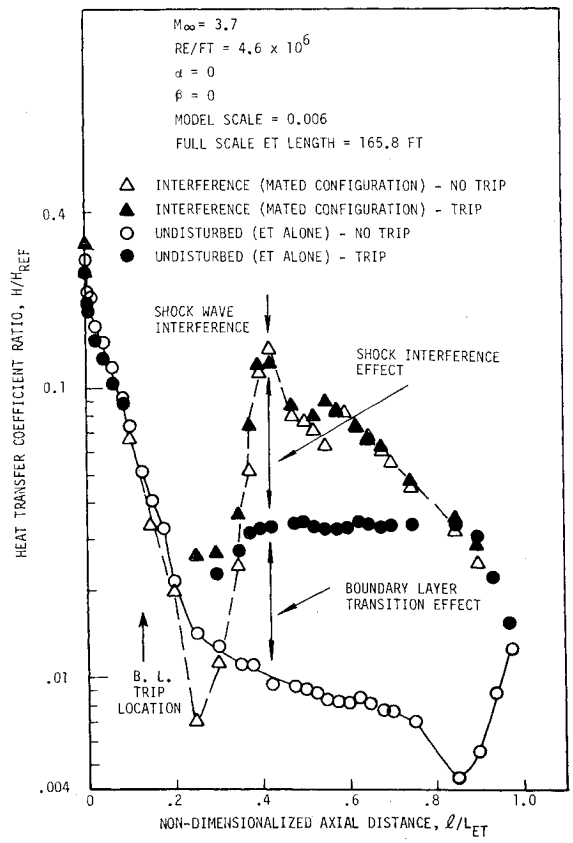

Fig. 16 Effect of boundary-layer trip on Space Shuttle external tank upper centerline heating.[2]

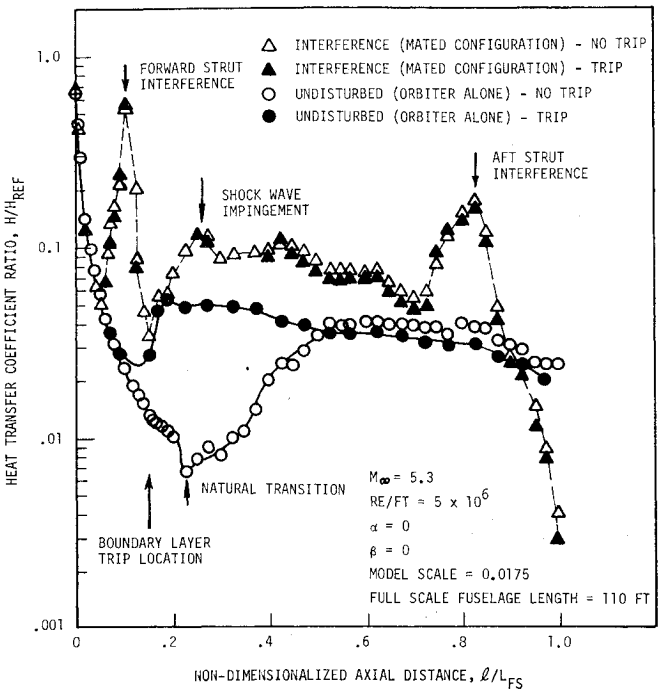

Fig. 17 Effect of boundary-layer trip on Space Shuttle Orbiter lower centerline heating.[2]

6) The simple correlation in Fig. 10 can be used to predict peak interference heating once the freestream flow conditions and wedge angle are specified. For laminar/laminar flows

$$ST^*_{i,PK(2)} = (C)0.332(Re^*_{x,PK(2)})^{-1/2}(Pr^*_{(2)})^{-2/3} \quad (5)$$

For the case of laminar/turbulent or turbulent/turbulent flow

$$ST^*_{i,PK(2)} = (C)0.0288(Re^*_{x,PK(2)})^{-1/5}(Pr^*_{(2)})^{-2/3} \quad (6)$$

where the constant, C, can have a value ranging from 1.0 to 2.0 as shown in Fig. 10. A conservative value of 2.0 should be used for thermal design purposes. The value of C is larger than one because of complex viscous-inviscid interaction effects whose analysis is beyond the scope of this paper.

The boundary-layer transition effect due to impinging shock waves can be used to explain the extremely high interference heating factors in Figs. 1, 3, and 4. All the experiments represented by these figures were repeated with boundary-layer trips installed on the flat plate near the leading edge, the orbiter nose, and the external tank nose. Results in Figs. 15-17 indicate that without the boundary-layer trips, the undistrubed flow is laminar, but flow transition occurs when the boundary-layer trips are installed. However, it is interesting to note that boundary-layer trips have no effect on peak interference heating values. This indicates that the flow in the interference region has already been tripped by the impinging shock wave even in the absence of a boundary-layer trip. Thus, the effect of a boundary-layer trip is actually to change the entire flow on the flat plate from laminar/turbulent to turbulent/turbulent. It should be emphasized that for the case of laminar/turbulent flow, a turbulent $H_{i,PK}$ should be ratioed to a turbulent H_u in order to derive meaningful turbulent heating factors. The large factors in Figs. 1, 3, and 4 are actually turbulent $H_{i,PK}$/laminar H_u values, which include both the shock-impingement effect (or the so-called pressure effect) and the boundary layer transition effect as shown in Figs. 15 and 16.

Finally, it is of interest to briefly compare this analysis with another interference heating prediction method that can be expressed as

$$H_{i,PK}/H_u = (P_{i,PK}/P_u)^n \quad (7)$$

where n varies from 0.7 to 0.85 depending on laminar or turbulent flow.[1,7,8,12,15] Equation (7) is well known with excellent correlation results. But the results of this study provide much more than just interference heating factors given by Eq. (7). The information of interference heating variation with Reynolds number, transition Reynolds number and effect of boundary-layer transition on interference heating derived in this study are not included in Eq. (7).

Conclusions

A simple method is developed to predict peak interference heating to a flat-plate surface under the influence of an impinging shock wave. Once a freestream flow condition and wedge angle are specified, peak interference heating can be computed for either laminar or turbulent oncoming flow with or without flow transition due to an impinging shock wave. The interference transition Reynolds number is also derived in this study. Finally, results of this study indicate that for the case of laminar/turbulent flow the extremely high interference heating factors are mostly due to boundary-layer transition.

References

[1] Haslett, R. A., Kaufman II, L. G., Romanowski, R. F., and Urkowitz, M., "Interference Heating Due to Shock Impingement," Air Force Flight Dynamics Lab, Wright-Patterson AFB, Ohio, AFF-DL-TR-72-66, July 1972.

[2] *Space Shuttle Aerodynamic Heating Data Book*, Rockwell International Corporation, Space Division, Downey, California, Vol. I., Feb. 1975, Vol. II., July 1975, Vol. III., May 1975.

[3] Murphy, J. D., "A Critical Evaluation of Analytic Methods for Predicting Laminar Boundary Layer Shock-Wave Interaction," NASA SP-228, Oct. 1969.

[4] Eckert, E. R. G., "Survey of Boundary Layer Heat Transfer at High Velocities and High Temperatures," Wright Air Development Center, Wright Patterson AFB, Ohio, WADC Technical Report 59-624, 1960.

[5] Spalding, D. B. and Chi, S. W., "The Drag of a Compressible Turbulent Boundary Layer on a Smooth Flat Plate with and without Heat Transfer," *Journal of Fluid Mechanics*, Vol. 18, Part 1, Jan. 1964, pp. 117-143.

[6] Monaghan, R. J., "On the Behavior of Boundary Layers at Supersonic Speeds," IAS-RAeS Proceedings – 1955.

[7] Hung, F. T., "Interference Heating Due to Shock Wave Impingement on Laminar Boundary Layers," AIAA Paper 73-678, Palm Springs, Calif., 1973.

[8] Sayano, S., "Heat Transfer in Shock Wave-Turbulent Boundary Layer Interaction Regions," Douglas Aircraft Co., Santa Monica, Rept. SM-42567, Nov. 1962.

[9] Levin, V. and Fabish, T. J., "Thermal Effects of Shock Wave-Turbulent Boundary Layer Interaction at Mach Numbers 3 and 5," North American Aviation, Downey, Calif., Rept. NA 62H-795, Nov. 1962.

[10] Gulbran, C. E., Redeker, E., Miller, D. S., and Strack, S. L., "Heating in Regions of Interference Flow Fields," The Boeing Company, Seattle, Wash., Technical Rept. AFFDL-TR-65-49, Part III, March 1967.

[11] Hung, F. T. and Scottoline, C. A., "Aerodynamic Heating in Gaps in the Presence of Protuberances and Shock Wave Impingement," AIAA Paper 75-670, Denver, Colo., 1975.

[12] Johnson, C. B. and Kaufman, L. G., "Interference Heating from Interactions of Shocks with Turbulent Boundary Layers at Mach 6," NASA TN D-7649, Sept. 1974.

[13] Magnan, J. D. and Spurlin, C. J., "Investigation of Flow Field Interference Caused by Shock Impingement on a Flat Plate at Mach Numbers of 6, 8, and 10," Arnold Engineering Development Center, Arnold AFB, Tenn., AEDC-TR-66-85, 1966.

[14] Kaufman, L. G. and Johsnon, C. B., "Weak Incident Shock Interactions with Mach 8 Laminar Boundary Layers," NASA TN D-7835, Dec. 1974.

[15] Holden, M. S., "Shock Wave-Turbulent Boundary Layer Interaction in Hypersonic Flow," AIAA Paper 72-74, San Diego, Calif., 1972.

[16] Pinckney, S. Z., "Data on Effects of Incident-Reflecting Shocks on the Turbulent Boundary Layer," NASA TM X-1221, March 1966.